Available online at www.sciencedirect.com
SCIENCE DIRECT®
Physica C 385 (2003) 66–74
PHYSICA C
www.elsevier.com/locate/physc

Anisotropic Eliashberg theory of MgB_2: T_c, isotope effects, superconducting energy gaps, quasiparticles, and specific heat

Hyoung Joon Choi [a], Marvin L. Cohen [a,b], Steven G. Louie [a,b,*]

[a] *Department of Physics, University of California at Berkeley, 366 LeConte Hall 7300, Berkeley, CA 94720-7300, USA*
[b] *Materials Sciences Division, Lawrence Berkeley National Laboratory, Berkeley, CA 94720, USA*

Abstract

The anisotropic Eliashberg formalism, employing results from the ab initio pseudopotential density functional calculations, is applied to study the superconducting properties of MgB_2. It is shown that the relatively high transition temperature of MgB_2 originates from strong electron–phonon coupling of the hole states in the boron σ-bonds although the coupling strength averaged over the Fermi surface is moderate, and the reduction of the isotope effect arises from the large anharmonicity of the relevant phonons. The superconducting energy gap is nodeless but its value varies strongly on different pieces of the Fermi surface. The gap values $\Delta(k)$ cluster into two groups at low temperature, a small value of ~2 meV and a large value of ~7 meV, resulting in two thresholds in the quasiparticle density of states and an increase in the specific heat at low temperature due to quasiparticle excitations over the small gap. All of these results are in good agreement with corresponding experiments and support the view that MgB_2 is a phonon-mediated multiple-gap superconductor.
© 2002 Published by Elsevier Science B.V.

PACS: 74.25.Jb; 74.25.B; 71.15.H
Keywords: Multi-gap superconductivity; Band structure; Isotope effect; Specific heat; Phonons; Eliashberg theory; Fermi surface

1. Introduction

MgB_2 is a readily available sp-bonded material for decades, but superconductivity for this material with a transition temperature of $T_c = 39$ K was discovered only very recently [1]. Subsequent experimental studies showed that this material not only has a much higher T_c than ordinary metallic superconductors, but also has significantly different superconducting properties [2–11]. The observed isotope effect is reduced substantially [2,3] from the BCS value of 1/2. The average electron–phonon coupling strength λ deduced from normal-state specific heat measurement [4–7] is found to be too small to justify the observed high T_c, using standard formula. In addition, specific heat measurements [4–7], tunneling [8] and photoemission [9] spectra, and point-contact spectroscopy [10,11] show low energy excitations suggesting a secondary energy gap.

To examine the superconductivity in MgB_2, theoretical calculations based on the BCS theory

* Corresponding author. Address: Department of Physics, University of California at Berkeley, 366 LeConte Hall 7300, Berkeley, CA 94720-7300, USA. Tel.: +1-510-642-1709; fax: +1-510-643-9473.
E-mail address: sglouie@uclink.berkeley.edu (S.G. Louie).

0921-4534/02/$ - see front matter © 2002 Published by Elsevier Science B.V.
PII: S0921-4534(02)02345-6

have been performed in great details using calculation of the electronic and phononic structures and the electron–phonon interactions [12–18]. MgB_2 is a metal with some hole states in the boron σ-bonds, and the Fermi surface consists of four distinctive pieces [12]. Large anharmonicity is found in the in-plane B–B stretching modes (E_{2g}) [13,14], and this anharmonicity is identified as the origin of the reduced isotope effect [13,15]. The electron–phonon coupling is dominated by the E_{2g} modes [12,15–17] and has strong variation on the Fermi surface [14,15,18]. This strong variation of the electron–phonon coupling on the Fermi surface is a key feature which must be properly considered to address the superconductivity of this material correctly [14,15,19].

The fully anisotropic Eliashberg formalism [20–22] is a suitable framework to describe the superconductivity in MgB_2 [15,19]. The strong momentum dependence of the superconducting energy gap is the origin of anomalies found in the quasiparticle density of states and the specific heat [19]. Here we describe the anisotropic Eliashberg formalism applied to MgB_2 and results for the transition temperature T_c, isotope-effect exponents α, momentum-dependent superconducting energy gap $\Delta(\mathbf{k})$, quasiparticle spectra, and specific heat. Electronic and phononic structures and electron–phonon interaction necessary for the Eliashberg equations are obtained by ab initio pseudopotential density functional calculations [23–26]. The large anharmonicity of some of the phonon frequencies is also considered in the equations. The results yield good agreement with corresponding experiments, providing a consistent physical picture that MgB_2 is a phonon-mediated superconductor with momentum-dependent values for the superconducting energy gap.

2. Anisotropic Eliashberg formalism

In this section, we present the anisotropic Eliashberg equations and formulas for the superconducting properties such as the transition temperature, the superconducting energy gap, the quasiparticle density of states, and the specific heat [20–22].

We start with the momentum-dependent Eliashberg function for nonnegative frequency ω which is defined by

$$\alpha^2F(\mathbf{k},\mathbf{k}',\omega) = N(\epsilon_F)\sum_j |\langle\mathbf{k}|\delta V_{\mathbf{q}}^j|\mathbf{k}'\rangle|^2\delta(\omega-\omega_{\mathbf{q}}^j). \tag{1}$$

Here $N(\epsilon_F)$ is the electron density of states per spin at the Fermi level, $|\mathbf{k}\rangle$ is the electronic state labeled by the crystal momentum $\mathbf{k}$, $\omega_{\mathbf{q}}^j$ is the phonon frequency for the branch j and the wave vector $\mathbf{q}=\mathbf{k}-\mathbf{k}'$, and $\delta V_{\mathbf{q}}^j$ is the difference of the total self-consistent crystal potential with and without a frozen phonon. In a self-consistent calculation with a frozen phonon, the atomic displacements are set to be $\langle 1j\mathbf{q}|\mathbf{x}|0j\mathbf{q}\rangle$ which is the expectation value of the atomic position operator $\mathbf{x}$ between the ground and the first excited phonon state. When we consider the phonon anharmonicity, $|0j\mathbf{q}\rangle$ and $|1j\mathbf{q}\rangle$ are the energy eigenstates of the atomic vibration in the anharmonic potential and $\omega_{\mathbf{q}}^j$ is the difference of their energy eigenvalues. The standard isotropic Eliashberg function $\alpha^2F(\omega)$ is given by

$$\alpha^2F(\omega) = \sum_{\mathbf{k},\mathbf{k}'} W_{\mathbf{k}}W_{\mathbf{k}'}\alpha^2F(\mathbf{k},\mathbf{k}',\omega), \tag{2}$$

where $W_{\mathbf{k}} = \delta(\epsilon_F-\epsilon_{\mathbf{k}})/N(\epsilon_F)$. The electron–phonon interaction functions $\lambda(\mathbf{k},\mathbf{k}',n)$, $\lambda(\mathbf{k},n)$, and $\lambda(n)$ for integral n and temperature T are

$$\lambda(\mathbf{k},\mathbf{k}',n) = \int_0^\infty d\omega\alpha^2F(\mathbf{k},\mathbf{k}',\omega)\frac{2\omega}{\omega^2+(2n\pi T)^2}, \tag{3}$$

$$\lambda(\mathbf{k},n) = \sum_{\mathbf{k}'} W_{\mathbf{k}'}\lambda(\mathbf{k},\mathbf{k}',n), \tag{4}$$

$$\lambda(n) = \sum_{\mathbf{k}} W_{\mathbf{k}}\lambda(\mathbf{k},n). \tag{5}$$

The standard electron–phonon coupling strength λ in the literature is $\lambda(n=0)$ in the above notation. Owing to the electron–phonon interaction, the electron density of states is increased by a factor of $(1+\lambda)$ from its bare value so that the electronic contribution to the specific heat at the normal state

is $C_N = \gamma_N T$ with $\gamma_N = (2/3)\pi^2 \times k_B^2 N(\epsilon_F)(1+\lambda)$. This formula for C_N is valid even when the electron–phonon interaction depends strongly on the momenta $\mathbf{k}$ and $\mathbf{k}'$.

We obtain the transition temperature from the Eliashberg equations. The anisotropic Eliashberg equations at imaginary frequency $i\omega_n = i(2n+1)\pi T$ are

$$Z(\mathbf{k}, i\omega_n) = 1 + \frac{1}{(2n+1)} \sum_{\mathbf{k}'n'} W_{\mathbf{k}'} \lambda(\mathbf{k}, \mathbf{k}', n-n') \times \frac{\omega_{n'}}{\sqrt{\omega_{n'}^2 + \Delta(\mathbf{k}', i\omega_{n'})^2}}, \tag{6}$$

$$Z(\mathbf{k}, i\omega_n)\Delta(\mathbf{k}, i\omega_n) = \pi T \sum_{\mathbf{k}'n'} W_{\mathbf{k}'} [\lambda(\mathbf{k}, \mathbf{k}', n-n') - \mu^*(\omega_c)] \times \frac{\Delta(\mathbf{k}', i\omega_{n'})}{\sqrt{\omega_{n'}^2 + \Delta(\mathbf{k}', i\omega_{n'})^2}}, \tag{7}$$

where the sum over the integer n' is truncated by a condition $|\omega_{n'}| < \omega_c$ for a given cutoff frequency ω_c. The dimensionless Coulomb pseudopotential $\mu^*(\omega)$ is defined by $\mu^*(\omega) = \mu/(1 + \mu \ln(\epsilon_F/\omega))$. At low enough temperature, Eqs. (6) and (7) have nonzero solution for $\Delta(\mathbf{k}, i\omega_n)$. As the temperature rises, the size of $\Delta(\mathbf{k}, i\omega_n)$ decreases. The transition temperature is the temperature that $\Delta(\mathbf{k}, i\omega_n)$ becomes zero.

In order to determine the superconducting energy gap, we need the gap function $\Delta(\mathbf{k}, \omega)$ for real frequency ω. This function can be obtained by an iterative analytic continuation [27] using

$$\omega Z(\mathbf{k}, \omega) = \omega + i\pi T \sum_{\mathbf{k}',n} W_{\mathbf{k}'} \lambda(\mathbf{k}, \mathbf{k}', \omega - i\omega_n) \times \frac{\omega_n}{\sqrt{\omega_n^2 + \Delta(\mathbf{k}', i\omega_n)^2}} + i\pi \sum_{\mathbf{k}'} W_{\mathbf{k}'} \int_{-\infty}^{\infty} d\omega' \times \frac{\alpha^2 F(\mathbf{k}, \mathbf{k}', \omega') Z(\mathbf{k}', \omega - \omega')(\omega - \omega')\Gamma(\omega, \omega')}{\sqrt{Z(\mathbf{k}', \omega - \omega')^2 [(\omega - \omega')^2 - \Delta(\mathbf{k}', \omega - \omega')^2]}}, \tag{8}$$

$$Z(\mathbf{k}, \omega)\Delta(\mathbf{k}, \omega) = \pi T \sum_{\mathbf{k}',n} W_{\mathbf{k}'} [\lambda(\mathbf{k}, \mathbf{k}', \omega - i\omega_n) - \mu^*(\omega_c)] \times \frac{\Delta(\mathbf{k}', i\omega_n)}{\sqrt{\omega_n^2 + \Delta(\mathbf{k}', i\omega_n)^2}} + i\pi \sum_{\mathbf{k}'} W_{\mathbf{k}'} \int_{-\infty}^{\infty} d\omega' \times \frac{\alpha^2 F(\mathbf{k}, \mathbf{k}', \omega') Z(\mathbf{k}', \omega - \omega')\Delta(\mathbf{k}', \omega - \omega')\Gamma(\omega, \omega')}{\sqrt{Z(\mathbf{k}', \omega - \omega')^2 [(\omega - \omega')^2 - \Delta(\mathbf{k}', \omega - \omega')^2]}} \tag{9}$$

where $\alpha^2 F(\mathbf{k}, \mathbf{k}', \omega) = -\alpha^2 F(\mathbf{k}, \mathbf{k}', -\omega)$ for $\omega < 0$, $\Gamma(\omega, \omega') = (\tanh((\omega - \omega')/2T) + \coth(\omega'/2T))/2$, and $\lambda(\mathbf{k}, \mathbf{k}', \omega - i\omega_n) = -\int_{-\infty}^{\infty} d\omega' \alpha^2 F(\mathbf{k}, \mathbf{k}'\omega')/(\omega - i\omega_n - \omega')$. The square roots are chosen to have positive imaginary parts. Once $\Delta(\mathbf{k}, \omega)$ is obtained, it is straightforward to obtain the superconducting gap and the quasiparticle density of states. The superconducting gap $\Delta(\mathbf{k})$ on the Fermi surface is the frequency ω satisfying

$$\omega = \mathrm{Re}[\Delta(\mathbf{k}, \omega)]. \tag{10}$$

The quasiparticle density of states $N(\omega)$ for the quasiparticle energy ω is

$$N(\omega) = N(\epsilon_F) \times \sum_{\mathbf{k}} W_{\mathbf{k}} \mathrm{Re}\left[\frac{(\omega + i\Gamma)}{\sqrt{(\omega + i\Gamma)^2 - \Delta(\mathbf{k}, \omega)^2}}\right] \tag{11}$$

with an assumed finite lifetime Γ of the quasiparticle.

We calculate the specific heat from the free energy. At temperature below T_c, the free energy difference $\Delta F = F_S - F_N$ between the superconducting and normal states [28] is

$$\Delta F = -\pi T N(\epsilon_F) \sum_{\mathbf{k}n} W_{\mathbf{k}} \left(\sqrt{\omega_n^2 + \Delta(\mathbf{k}, i\omega_n)^2} - |\omega_n|\right) \times \left(Z(\mathbf{k}, i\omega_n) - Z^N(\mathbf{k}, i\omega_n)|\omega_n| \Big/ \sqrt{\omega_n^2 + \Delta(\mathbf{k}, i\omega_n)^2}\right), \tag{12}$$

where $Z^N(\mathbf{k}, i\omega_n)$ are the values of $Z(\mathbf{k}, i\omega_n)$ of Eq. (6) with $\Delta(\mathbf{k}', i\omega_{n'}) = 0$. Then, the specific heat difference $\Delta C = C_S - C_N$ between the superconducting and normal states is

$$\Delta C = -T\frac{d^2\Delta F}{dT^2}. \quad (13)$$

If we neglect all the **k** dependencies and the sum over **k** in the above equations and formulas, we obtain the isotropic Eliashberg formalism. If the electron–phonon interaction did not depend strongly on the electronic states on the Fermi surface, the isotropic formalism would be an appropriate approximation.

3. Electronic and phononic structures and electron–phonon interaction

The electronic structure of MgB_2 is calculated using ab initio pseudopotentials [23,24] with the local density approximation to the density functional theory. We used a $12 \times 12 \times 12$ k-point grid in the Brillouin zone (BZ) for self-consistent calculations and a $18 \times 18 \times 12$ grid for the Fermi surface properties, and included planewaves up to 60 Ry as a basis to expand the electronic wavefunctions. The calculated equilibrium lattice constants are $a = 3.071$ Å and $c = 3.578$ Å, in good agreement with measured values [1]. Fig. 1 shows the band structure of MgB_2 along the symmetry lines of the BZ. We have both σ- and π-bonding boron bands at the Fermi level. The Fermi surface consists of four sheets; the σ-bands form two holelike coaxial cylinders along Γ to A line, and the π-bands form a holelike tubular network near K and M, and an electron like tubular network near H and L. The density of states at the Fermi energy is 0.12 states/eV atom spin, 44% of which comes from the σ-bonds and the other 56% comes from the π-bonds.

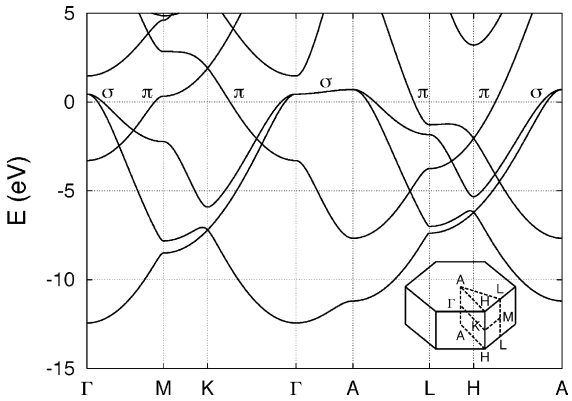

Fig. 1. Electronic structure of MgB_2. Inset: BZ of the simple hexagonal structure.

Phonon frequencies and electron–phonon interactions are obtained from the frozen phonon calculations [25,26] at all the symmetry points of the BZ. To account for the phonon anharmonicity, the variation of the total energy with a frozen phonon amplitude is fitted with a fourth order polynomial, and then the energy difference of the ground and the first excited vibrational state is regarded as the anharmonic phonon frequency. For the harmonic phonon frequency, we considered only the quadratic term of the fitted total-energy curve. In the case of the doubly degenerate, in-plane B–B stretching modes (E_{2g}) at Γ and A, we calculate the two-dimensional vibrational states after the total energy is fitted in a plane with $E(r,\theta) = E_0 + c_2r^2 + c_2r^4 + (c_3r^3 + c_5r^5)\cos(3\theta)$. We use natural atomic weights for B and Mg, that is, 10.81 for B and 24.31 for Mg. The electron–phonon interaction is calculated from $\delta V_{\mathbf{q}}^j$ as described in Eq. (1). Phonon frequencies and $\delta V_{\mathbf{q}}^j$ are obtained in a $18 \times 18 \times 12$ grid in the BZ by interpolation [15]. All calculations are done twice for comparison: one with harmonic phonon frequencies and another with anharmonic phonon frequencies. To study the isotope effect, we repeat the entire procedure with an isotopic atomic mass.

Fig. 2 shows the phonon dispersion along the symmetry lines of the BZ. Only the in-plane B–B stretching modes (E_{2g}) along the Γ to A line have large anharmonicity. The calculated anharmonic frequency, 75.9 meV, for the E_{2g} mode at Γ agrees very well with the results from Raman measurements [29,30] as well as other theoretical calculations [13,14]. Fig. 3 shows the phonon density of states $F(\omega)$ and the standard Eliashberg function $\alpha^2F(\omega)$. The large dominant peak in $\alpha^2F(\omega)$ at 63 meV in the harmonic case or 77 meV in the anharmonic case arises from the E_{2g} modes. The E_{2g} modes have large electron–phonon coupling with the σ-bonding boron bonds within a small volume in k-space along the Γ to A line, within the harmonic approximation, the isotropic

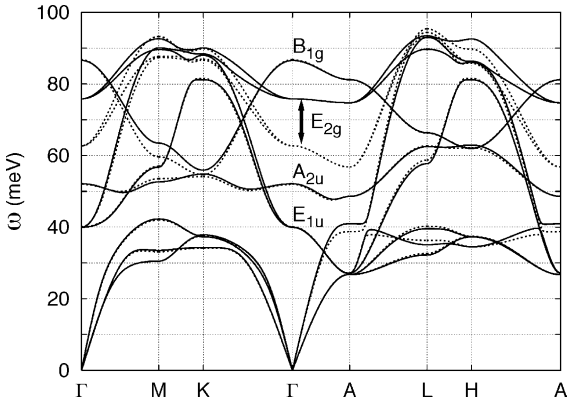

Fig. 2. Calculated phonon dispersion in MgB_2. Solid lines represent the anharmonic phonon frequencies which are obtained from the energy difference of the ground and the first excited state of the atomic vibrations. Dotted lines represent the standard harmonic phonon frequencies. The frequencies are obtained along the symmetry lines by interpolation from the exact results at the symmetry points. For more precise dispersions in between the symmetry points in the harmonic case, see Refs. [17,18].

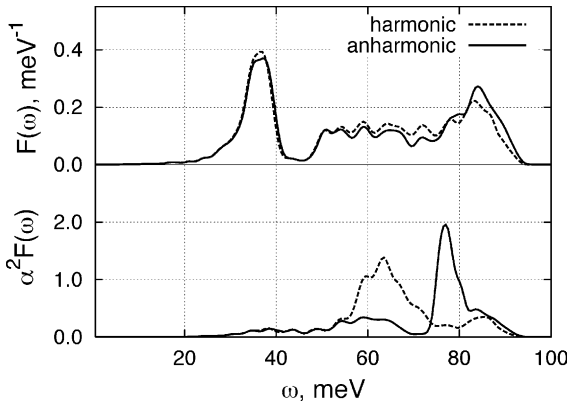

Fig. 3. Phonon density of states $F(\omega)$ and the isotropic Eliashberg function $\alpha^2F(\omega)$ for MgB_2. (After Ref. [15].)

average electron–phonon coupling constant, $\lambda = 2\int d\omega\alpha^2F(\omega)/\omega$, is 0.73 and the logarithmic average frequency, $\omega_{\ln} = \exp[(2/\lambda)\int d\omega\alpha^2F(\omega)\ln\omega/\omega]$, is 59.4 meV. With anharmonicity, λ is reduced to 0.61 and $\omega_{\ln}$ is increased to 63.5 meV. The reduced value of $\lambda = 0.61$ due to anharmonicity corresponds to $\gamma_N = 2.6$ mJ/mol K^2 in our calculation. This value agrees very well with result from specific heat measurements [4,5], showing that the electron–phonon interaction is weakened by phonon anharmonicity in MgB_2. This value of $\lambda = 0.61$ is too small to explain a T_c of 39 K using either the McMillan [31] or the Allen-Dynes [32] formula. This will be discussed further in the next section.

Fig. 4 shows the variation of the calculated electron–phonon interaction on the Fermi surface. The mass enhancement factor $\lambda(\mathbf{k}, n = 0)$ for states at $\mathbf{k}$ in Fig. 4(a) shows two well-separated sets of values: about 0.8–1.0 on the σ sheets and about 0.3–0.5 on the π sheets. For more detail, we depict in Fig. 4(b) the values of $\lambda(\mathbf{k} = \mathbf{k}_0, \mathbf{k}', n = 0)$ as a function of $\mathbf{k}'$ for a fixed $\mathbf{k} = \mathbf{k}_0$ on the Fermi surface near Γ. The interaction function $\lambda(\mathbf{k}, \mathbf{k}', n)$ defined by Eq. (3) represents the strength for a pair of electrons at states $\mathbf{k}$ and $-\mathbf{k}$ scattering to $\mathbf{k}'$ and $-\mathbf{k}'$ by phonon exchange. The plot in Fig. 4(b) shows strong and varying strength for scattering from the σ sheets onto the σ sheets but rather weak strength for scattering to the π sheets. Fig. 5 shows the number density of $(\mathbf{k}, \mathbf{k}')$ pairs on the Fermi surface plotted as a function of the value of $\lambda(\mathbf{k}, \mathbf{k}', n = 0)$. The coupling strength $\lambda(\mathbf{k}, \mathbf{k}', n = 0)$

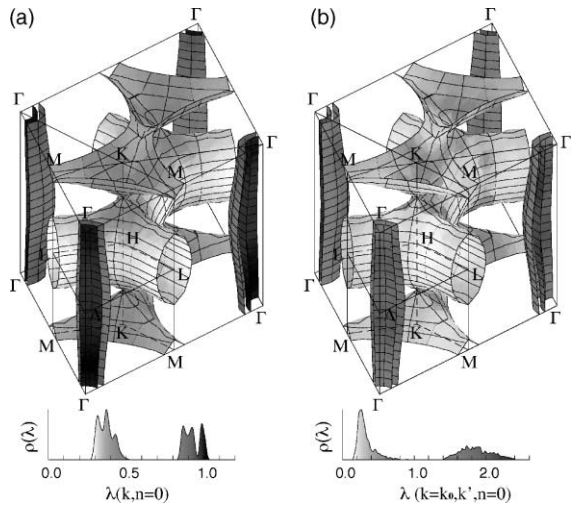

Fig. 4. Variation of the electron–phonon interaction λ on the Fermi surface of MgB_2. (a) The mass enhancement factor $\lambda(\mathbf{k}, n = 0)$ is shown in a gray scale and (b) the electron–phonon interaction function $\lambda(\mathbf{k} = \mathbf{k}_0, \mathbf{k}', n = 0)$ is given in a gray scale as a function of $\mathbf{k}'$ for a fixed $\mathbf{k}_0$ on the Fermi surface near Γ. (After Ref. [15].)

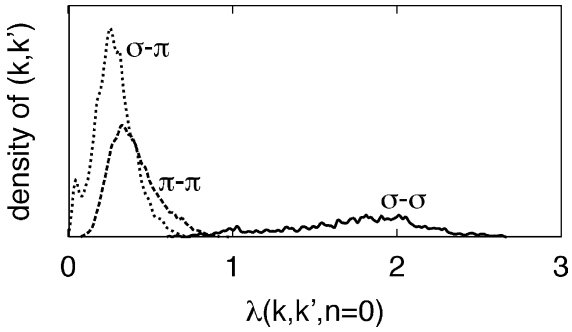

Fig. 5. Number density of $(\mathbf{k}, \mathbf{k}')$ pairs on the Fermi surface versus the value of $\lambda(\mathbf{k}, \mathbf{k}', n = 0)$. The number density is split into three sets: both $\mathbf{k}$ and $\mathbf{k}'$ are on the two σ cylindrical sheets of the Fermi surface (—), both on the two π tubular sheets (- - -), and one on a σ cylindrical sheet and the other on a π tubular sheet (· · ·). (After Ref. [15].)

between states on the σ sheets has values exceeding 2.0 which is much larger than those within the π sheets or between a σ sheet and a π sheet. This strong variation of electron–phonon interaction in MgB_2 can be considered properly with the anisotropic Eliashberg formalism of the previous section.

4. Transition temperature and isotope effect

We calculate the transition temperature of MgB_2 from the fully anisotropic Eliashberg equations. The anisotropic Eliashberg equations at the imaginary frequency, Eqs. (6) and (7), are constructed and the transition temperature is calculated as described in Section 2. The cutoff frequency ω_c is set to 0.5 eV which is about six times larger than the maximum phonon frequency. With the exception of $\mu^*(\omega_c)$, our calculation of the phonon frequencies and electron–phonon interaction provides all the material parameters for the Eliashberg equation. We use the anharmonic phonon frequencies defined in Sections 2 and 3 for the phonon frequencies $\omega_{\mathbf{q}}^j$ in the equations. The dimensionless Coulomb pseudopotential $\mu^*(\omega)$ is known to be of order 0.1 in most metals when ω is a relevant phonon frequency [22,31,33].

The obtained transition temperature is in the range of $42\ \mathrm{K} \geqslant T_c \geqslant 37\ \mathrm{K}$ for $0.10 \leqslant \mu^*(\omega_c) \leqslant 0.14$. In particular, T_c is 39 K when $\mu^*(\omega_c) = 0.12$. This value of $\mu^*(\omega_c) = 0.12$ corresponds to $\mu^*(\omega_{\ln}) = 0.10$ with $\omega_{\ln} = 63.5$ meV obtained in Section 3. For comparison, if we neglect the anisotropy and calculate T_c with the isotropic Eliashberg equations, T_c drops to 19 K. This shows clearly that the strong variation in the electron–phonon coupling on the Fermi surface is crucial to the observed high T_c in MgB_2. In MgB_2, therefore, an average electron–phonon coupling λ cannot be correctly determined from T_c using the McMillan [31] or Allen-Dynes formulas [32] because these formulas are based on the isotropic Eliashberg equations. However, a determination of λ from the specific heat measurement is still valid. This explains the apparent discrepancy between the values of λ estimated from specific heat measurements and λ estimated from T_c using simplified isotropic models.

To calculate the isotope-effect exponent α ($T_c \propto M^{-\alpha}$), we recalculate T_c using the mass of either ^{10}B or ^{26}Mg in place of the natural atomic weight. We obtain $\alpha_B = 0.32$ and $\alpha_{Mg} = 0.03$ from the anisotropic Eliashberg equation with anharmonic phonon frequencies. These values are very close to the experimental values $\alpha_B = 0.26$–0.30 and $\alpha_{Mg} = 0.02$ [2,3]. Without anharmonicity, we obtain $\alpha_B = 0.46$ and $\alpha_{Mg} = 0.02$. Hence, the anomalously low isotope-effect exponent is primarily due to phonon anharmonicity.

5. Superconducting energy gap, quasiparticle spectra, and specific heat

We solve the anisotropic Eliashberg equations, Eqs. (6) and (7), at low temperature, and obtain the gap function $\Delta(\mathbf{k}, \omega)$ for real frequency ω using Eqs. (8) and (9). The superconducting energy gap $\Delta(\mathbf{k})$ on the Fermi surface is then calculated by Eq. (10). Fig. 6 shows the calculated superconducting energy gap $\Delta(\mathbf{k})$ at 4 K. When calculating the energy gap, we did not make any assumption on its functional shape on the Fermi surface. The resulting superconducting energy gap is nodeless and always of the same sign, but the size of the gap changes greatly on the different pieces of the Fermi surface. The magnitude of the energy gap at 4 K

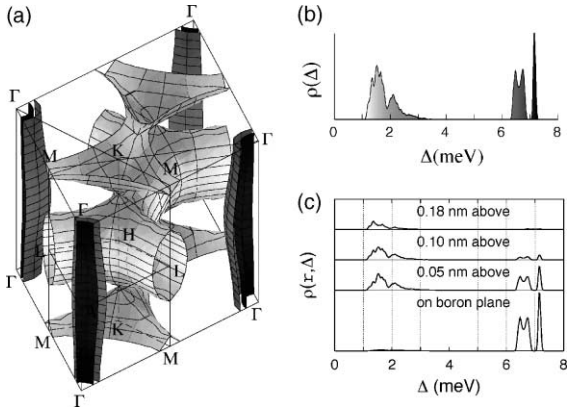

Fig. 6. The superconducting energy gap of MgB_2. (a) The superconducting energy gap on the Fermi surface at 4 K is given in a gray scale, (b) the distribution of gap values at 4 K and (c) local distribution of the superconducting energy gap is plotted on a boron plane and on planes at 0.05, 0.10, and 0.18 nm above a boron plane, respectively. (After Ref. [19].)

ranges from 6.4 to 7.2 meV on the σ sheets, and from 1.2 to 3.7 meV on the π sheets. The average values of the gap are 6.8 meV for the σ sheets and 1.8 meV for the π sheets. Our result is consistent with the recent experiments reporting two gaps [4,5,7–10,34,35]. The variation of the superconducting energy gap on the Fermi surface is directly measurable by techniques such as high resolution angle-resolved photoelectron spectroscopy.

Fig. 6(c) shows a local gap distribution defined by $\rho(\mathbf{r}, \Delta) = \Sigma_{\mathbf{k}} |\psi_{\mathbf{k}}(\mathbf{r})|^2 \delta(\Delta - \Delta(\mathbf{k}))$, where $\psi_{\mathbf{k}}(\mathbf{r})$ is the electron wave function with crystal momentum $\mathbf{k}$. Since the σ-bonding states are confined to the boron planes, the strong pairing gap of around 6.8 meV is associated with these planes. In tunneling experiments along the c-axis, the small gaps should be seen preferentially, as indicated in some recent measurements [8,10].

The superconducting energy gap is calculated at various temperatures. Fig. 7(a) shows the distribution of the energy gap values. Vertical solid curves represent the distribution of the superconducting gap values at various temperatures from 4 to 38 K. Dashed curves are of the form $\Delta(T) = \Delta(0)(1 - (T/T_c)^p)^{1/2}$ fitted separately to the calculated average energy gap of the σ-bonding states and that of the π-bonding states. For the σ-bonding states, $\Delta(0) = 6.8$ meV $(2\Delta(0)/k_B T_c = 4.0)$ and $p = 2.9$. For the π-bonding states, $\Delta(0) = 1.8$ meV $(2\Delta(0)/k_B T_c = 1.06)$ and $p = 1.8$. Thus, the energy gap of the σ-bonding states and that of the π-bonding states show different temperature dependence. Compared with the small energy gap of the π-bonding states, the large energy gap of the σ-bonding states changes more slowly at low temperature, but more rapidly near the transition temperature. Both the π and σ gaps vanish at the same transition temperature although their values are greatly different at low temperature [36]. This temperature dependence of the superconducting energy gaps agree with recent tunneling, optical, and specific heat measurements [4,5,7–10,34].

Fig. 7(b) shows the quasiparticle density of states calculated with Eq. (11) and an assumed finite lifetime Γ of 0.1 meV. Since the energy gap differs considerably for the σ- and π-bonding states in MgB_2, the density of quasiparticle excitations as a function of energy shows two thresholds: one for quasiparticle excitations of π-bonding states and the other for those of σ-bonding states. The quasiparticle density of states can be deduced experimentally from tunneling experiments and

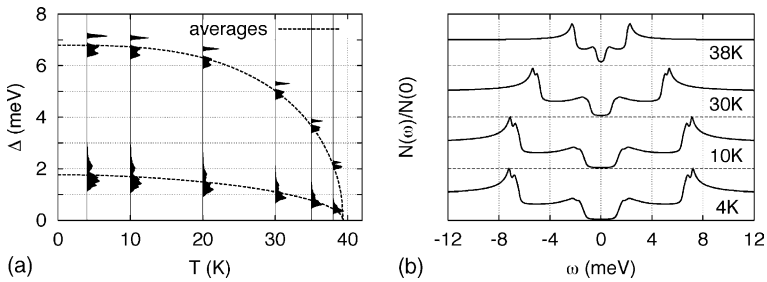

Fig. 7. Calculated temperature dependence of (a) the superconducting gaps and (b) the quasiparticle density of states. (After Ref. [19].)

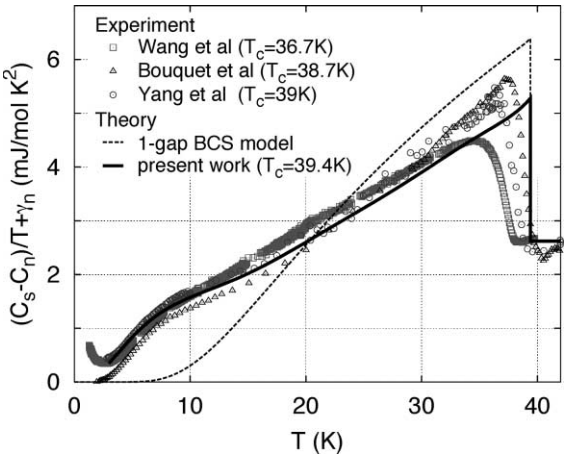

Fig. 8. The specific heat of MgB_2. The solid curve represents the result of our theoretical calculation. Symbols are the results of experimental measurements [4,5,7] and the dashed curve is the standard 1-gap BCS prediction corresponding to a transition temperature of 39.4 K. (After Ref. [19].)

various spectroscopic measurements [8–10,34], but a direct quantitative comparison requires knowledge of various physical parameters involved in a specific experiment.

We calculate the specific heat of the superconducting state from the free energy [28] using Eqs. (12) and (13). Fig. 8 shows the measured and calculated electronic contribution to the specific heat of MgB_2 as a function of temperature. The measured specific heat [4,5,7] of MgB_2 at low temperature is substantial and a large hump appears at about 10 K which is inconsistent with a 1-gap BCS model. As shown in Fig. 8, the overall shape and magnitude of our calculated specific heat curve agrees very well with the experimental data, especially below 30 K. We find that the low temperature hump in our calculated curve and in the experimental data is caused by the existence of low energy excitations across the small superconducting energy gap of the π-bonding states.

6. Conclusion

We have shown that in MgB_2 the anisotropy of the electron–phonon interaction on the Fermi surface is strong enough to raise T_c to 39 K even though the interaction is weakened by the anharmonicity of the phonons as compared to the harmonic case. The boron isotope-effect exponent α_B is reduced from almost 0.5 to 0.32 because of the anharmonicity of the phonons. The size of superconducting energy gap varies strongly on the Fermi surface so that the gap values $\Delta(\mathbf{k})$ cluster into two groups—a small value of $\sim$2 meV and a large value of $\sim$7 meV. This large variation of the superconducting energy gap produces anomalies in the quasiparticle density of states and the specific heat of the superconducting states. Our study shows that the phonon-mediated electron pairing theory describes the superconductivity in MgB_2 successfully as long as both the anisotropy of the electron–phonon interaction and the anharmonicity of the phonons are properly taken into account. With the success of the anisotropic Eliashberg theory presented here, we expect that a proper extension of the theory with applied magnetic field will describe the magnetic properties of MgB_2 successfully.

Acknowledgements

We would like to thank David Roundy and Hong Sun for collaborations of the work reviewed here. This work was supported by National Science Foundation grant no. DMR00-87088, and by the Director, Office of Science, Office of Basic Energy Sciences of the US Department of Energy under contract DE-AC03-76SF00098. Computational resources have been provided by the National Science Foundation at the National Center for Supercomputing Applications and by the National Energy Research Scientific Computing Center. H.J.C. acknowledges support from the Miller Institute for Basic Research in Science.

References

[1] J. Nagamatsu, N. Nakagawa, T. Muranaka, Y. Zenitani, J. Akimitsu, Nature 410 (2001) 63.
[2] S.L. Bud'ko, G. Lapertot, C. Petrovic, C.E. Cunningham, N. Anderson, P.C. Canfield, Phys. Rev. Lett. 86 (2001) 1877.
[3] D.G. Hinks, H. Claus, J.D. Jorgensen, Nature 411 (2001) 457.

[4] Y. Wang, T. Plackowski, A. Junod, Physica C 355 (2001) 179.
[5] F. Bouquet, R.A. Fisher, N.E. Phillips, D.G. Hinks, J.D. Jorgensen, Phys. Rev. Lett. 87 (2001) 47001.
[6] F. Bouquet, Y. Wang, R.A. Fisher, D.G. Hinks, J.D. Jorgensen, A. Junod, N.E. Phillips, Europhys. Lett. 56 (2001) 856.
[7] H.D. Yang, J.-Y. Lin, H.H. Li, F.H. Hsu, C.J. Liu, S.-C. Li, R.-C. Yu, C.-Q. Jin, Phys. Rev. Lett. 87 (2001) 167003.
[8] F. Giubileo, D. Roditchev, W. Sacks, R. Lamy, D.X. Thanh, J. Klein, S. Miraglia, D. Fruchart, J. Marcus, Ph. Monod, Phys. Rev. Lett. 87 (2001) 177008.
[9] S. Tsuda, T. Yokoya, T. Kiss, Y. Takano, K. Togano, H. Kito, H. Ihara, S. Shin, Phys. Rev. Lett. 87 (2001) 177006.
[10] P. Szabó, P. Samuely, J. Kačmarčík, T. Klein, J. Marcus, D. Fruchart, S. Miraglia, C. Marcenat, A.G.M. Jansen, Phys. Rev. Lett. 87 (2001) 137005.
[11] F. Laube, G. Goll, J. Hagel, H.V. Lohneysen, D. Ernst, T. Wolf, cond-mat/0106407 (2001).
[12] J. Kortus, I.I. Mazin, K.D. Belashchenko, V.P. Antropov, L.L. Boyer, Phys. Rev. Lett. 86 (2001) 4656.
[13] T. Yildirim, O. Gülseren, J.W. Lynn, C.M. Brown, T.J. Udovic, Q. Huang, N. Rogado, K.A. Regan, M.A. Hayward, J.S. Slusky, T. He, M.K. Haas, P. Khalifah, K. Inumaru, R.J. Cava, Phys. Rev. Lett. 87 (2001) 37001.
[14] A.Y. Liu, I.I. Mazin, J. Kortus, Phys. Rev. Lett. 87 (2001) 87005.
[15] H.J. Choi, D. Roundy, H. Sun, M.L. Cohen, S.G. Louie, Phys. Rev. B 66 (2002) 020513.
[16] J.M. An, W.E. Pickett, Phys. Rev. Lett. 86 (2001) 4366.
[17] K.-P. Bohnen, R. Heid, B. Renker, Phys. Rev. Lett. 86 (2001) 5771.
[18] Y. Kong, O.V. Dolgov, O. Jepsen, O.K. Andersen, Phys. Rev. B 64 (2001) 020501.
[19] H.J. Choi, D. Roundy, H. Sun, M.L. Cohen, S.G. Louie, Nature 418 (2002) 758.
[20] G.M. Eliashberg, Zh. Eksp. Teor. Fiz. 38 (1960) 966; Sov. Phys.—JETP (Engl. Transl.) 11 (1960) 696.
[21] P.B. Alien, B. Mitrović, in: H. Ehrenreich, F. Seitz, D. Turnbull (Eds.), Solid State Physics, 37, Academic, New York, 1982, p. 1, references therein.
[22] J.P. Carbotte, Rev. Mod. Phys. 62 (1990) 1027.
[23] N. Troullier, J.L. Martins, Phys. Rev. B 43 (1991) 1993.
[24] J. Ihm, A. Zunger, M.L. Cohen, J. Phys. C 12 (1979) 4409.
[25] P.K. Lam, M.L. Cohen, Phys. Rev. B 25 (1982) 6139.
[26] M.M. Dacorogna, M.L. Cohen, P.K. Lam, Phys. Rev. Lett. 55 (1985) 837.
[27] F. Marsiglio, M. Schossmann, J.P. Carbotte, Phys. Rev. B 37 (1988) 4965.
[28] J. Bardeen, M. Stephen, Phys. Rev. 136 (1964) A1485.
[29] J. Hlinka, I. Gregora, J. Pokorný, A. Plecenik, P. Kúš, L. Satrapinsky, Š. Beňačka, Phys. Rev. B 64 (2001) 140503.
[30] A.F. Goncharov, V.V. Struzhkin, E. Gregoryanz, J. Hu, R.J. Hemley, H.-k. Mao, G. Lapertot, S.L. Bud'ko, P.C. Canfield, Phys. Rev. B 64 (2001) 100509.
[31] W.L. McMillan, Phys. Rev. 167 (1968) 331, and references therein.
[32] P.B. Allen, R.C. Dynes, Phys. Rev. B 12 (1975) 905.
[33] P. Morel, P.W. Anderson, Phys. Rev. 125 (1962) 1263.
[34] X.K. Chen, M.J. Konstantinovi, J.C. Irwin, D.D. Lawrie, J.P. Franck, Phys. Rev. Lett. 87 (2001) 157002.
[35] C. Buzea, T. Yamashita, Supercond. Sci. Technol. 14 (2001) R115, and references therein.
[36] H. Suhl, B.T. Matthias, L.R. Walker, Phys. Rev. Lett. 3 (1959) 552.